

---

# DISTILLING TEXTUAL PRIORS FROM LLM TO EFFICIENT IMAGE FUSION

---

**Ran Zhang, Liu Liu**

Hefei University of Technology  
Hefei, China

2023212219@mail.hfut.edu.cn, liuliu@hfut.edu.cn

**Xuanhua He, Ke Cao, Li Zhang, Man Zhou**

University of Science and Technology of China  
Hefei, China

hexuanhua@mail.ustc.edu.cn, caoke200820@mail.ustc.edu.cn,  
zanly20@mail.ustc.edu.cn, manman@mail.ustc.edu.cn

**Jie Zhang**

Hefei Institutes of Physical Science, Chinese Academy of Sciences  
Hefei, China

zhangjie@iim.ac.cn

## ABSTRACT

Multi-modality image fusion aims to synthesize a single, comprehensive image from multiple source inputs. Traditional approaches, such as CNNs and GANs, offer efficiency but struggle to handle low-quality or complex inputs. Recent advances in text-guided methods leverage large model priors to overcome these limitations, but at the cost of significant computational overhead, both in memory and inference time. To address this challenge, we propose a novel framework for distilling large model priors, eliminating the need for text guidance during inference while dramatically reducing model size. Our framework utilizes a teacher-student architecture, where the teacher network incorporates large model priors and transfers this knowledge to a smaller student network via a tailored distillation process. Additionally, we introduce spatial-channel cross-fusion module to enhance the model's ability to leverage textual priors across both spatial and channel dimensions. Our method achieves a favorable trade-off between computational efficiency and fusion quality. The distilled network, requiring only 10% of the parameters and inference time of the teacher network, retains 90% of its performance and outperforms existing SOTA methods. Extensive experiments demonstrate the effectiveness of our approach. Codes are available at <https://github.com/Zirconium233/DTPF>

**Keywords** Image Fusion · Knowledge Distillation · Large Language Models · Multi-modality Learning

## 1 Introduction

Image fusion plays a important role in visual enhancement within digital image processing. For example, visible-infrared image fusion combines color-based details from visible images, which are easily interpretable by humans, with radiation-based features from infrared images, which are highly effective for target detection and operations under low-light conditions. By integrating complementary information from both modalities, this fusion method produces high-quality images that enhance both human visual interpretation and machine-based detection performance.

During the imaging process, environmental and device-related constraints often degrade the quality of source images. Visible images may suffer from low resolution, while infrared images are prone to various noise types. Traditional fusion methods, including FusionGAN [1], U2Fusion [2], and SwinFusion [3], fuse source images without effectively

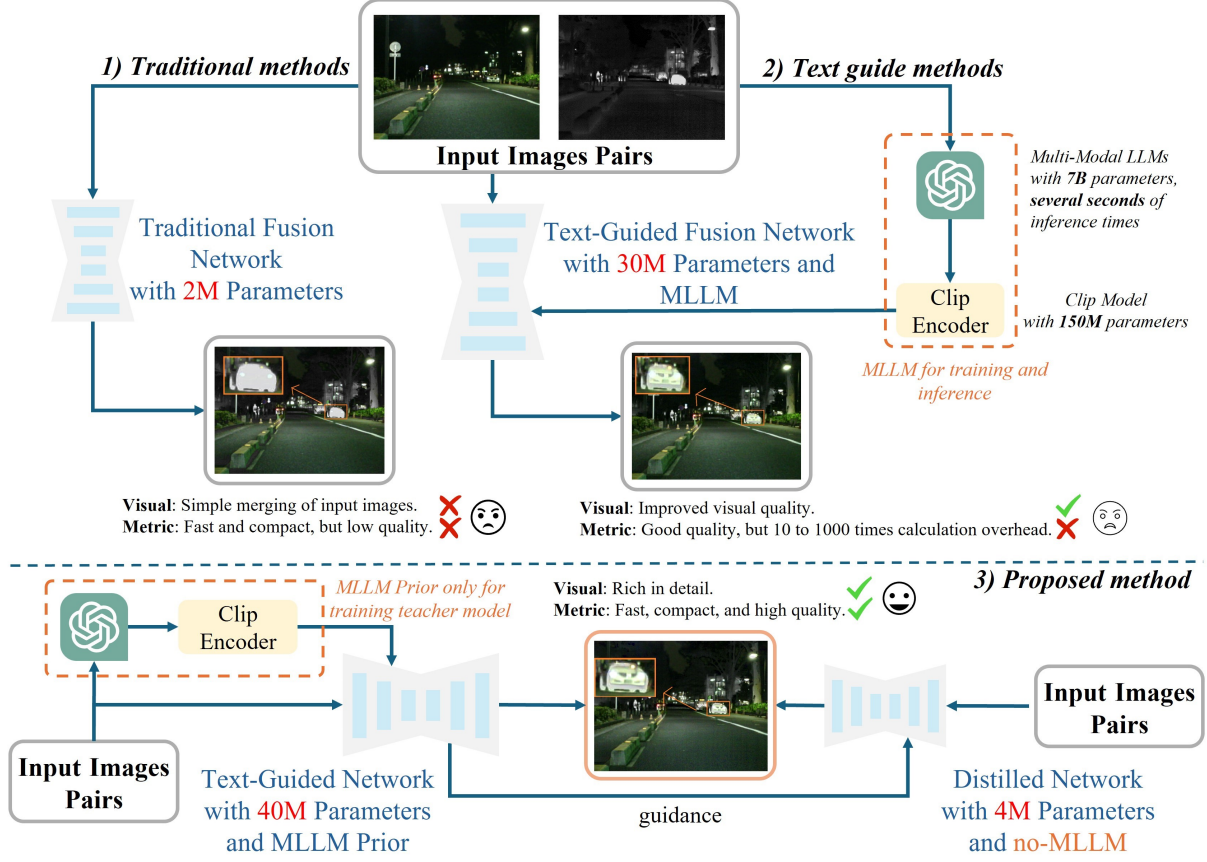


Figure 1: Overview of different image fusion methods and their parameter efficiency. (1) Traditional methods use small fusion networks. (2) Text-guided methods significantly increasing computational demands with performance improvements. (3) Our proposed method leverages text-guided training and knowledge distillation to create a distilled network that achieves high-quality fused images without relying on LLMs during inference.

distinguishing between degraded information and meaningful image content, leading to suboptimal performance. Some approaches [4] mitigate these issues by relying on manual pre-processing to enhance source images, but their flexibility is limited. Recently, text-guided methods, such as TextFusion and Text-IF [5], have emerged as a promising solution to address these challenges. These methods leverage the capabilities of multimodal large language models (MLLMs) to generate text captions or degradation descriptions (e.g., low light) for source images, enabling the model to adaptively distinguish image content from degradation and enhance image quality. By integrating these priors, the model gains enhanced semantic understanding of the image content, which effectively promote the fusion processes. For instance, Text-IF utilizes MLLMs [6] to generate task lists and incorporates CLIP [7] to guide the fusion process based on these descriptions. Similarly, TextFusion [8] employs text-based interactions to build models capable of focusing specific image elements, such as emphasizing trees over people, based on captions generated by LLMs or human input.

Despite their advantages, incorporating LLMs into the fusion workflow introduces significant resource overhead. In most cases, users aim to fuse images for downstream tasks such as detection or segmentation, without the need for extensive interaction. LLMs dramatically increase computational demands, often occupying ten to thousands of times more resources than the fusion module itself. Even CLIP, a relatively lightweight vision-language model, requires approximately five times the parameters of the fusion module. This computational cost makes LLMs disproportionate to the task. Moreover, due to the limitations in the quality and quantity of datasets, the performance gains from integrating large models are marginal compared to the significant decrease in efficiency. Thus, we seek a method that enables the model to perform degradation-aware fusion and enhances semantic understanding without relying on large-scale models.

In response to these issues, we propose a large-model prior distillation framework that eliminates the need for text guidance during inference while significantly reducing model size, as shown in Figure 1. Our framework employs a teacher-student architecture, where the teacher network integrates MLLM priors via a feature modulation operations.

To fully exploit textual priors across both spatial and channel dimensions, we introduce spatial-channel cross-fusion module (SCFM). A specially tailored prior distillation loss is then used to transfer textual knowledge from both feature and output perspectives, enabling the student network to mimic the teacher’s feature processing without requiring textual inputs. By leveraging this approach, our method achieves a 90% reduction in model size (excluding CLIP, which alone requires five times the parameters of the original fusion module) while retaining 90% of the teacher model’s performance.

Our contributions are summarized as follows:

- We propose a novel teacher-student framework to distill textual information from MLLMs and enhance the image fusion process without interfering with inference. A tailored prior distillation loss transfers knowledge from the teacher network to the student, enabling the student network to internalize textual information while reducing model size.
- We introduce spatial-channel cross fusion module to fully exploit textual information across both spatial and channel dimensions, improving the model’s ability to leverage textual priors.
- Extensive experiments on multiple datasets demonstrate that our method achieves state-of-the-art (SOTA) performance. Ablation studies further validate the effectiveness of our approach, highlighting its ability to achieve an optimal balance between efficiency and performance while providing valuable insights into model compression and the utilization of prior information.

## 2 Related Works

**Image fusion** has been a well-explored research area, and significant progress has been achieved with the advancements in deep learning. Early methods primarily utilized CNNs [2] to fuse images from different modalities. Subsequently, generative models [1, 9] and Transformer-based approaches [3, 10] were introduced to enhance fusion quality. Additionally, high-level vision tasks, such as object detection, have been incorporated to guide the fusion process [11]. However, these methods often overlook the degradation present in source images, resulting in suboptimal performance. To address this limitation, recent works, such as Text-IF [5] and Text-Fusion [8], leverage large model priors to achieve degradation-aware fusion. While effective, these approaches introduce substantial computational overhead, limiting their practicality for real-world applications.

**Knowledge distillation** has gained prominence as a strategy for compressing deep neural networks by transferring knowledge from a large “teacher” model to a smaller “student” model. This approach was initially popularized for reducing the computational overhead of deploying models on resource-constrained devices [12]. Distillation techniques include output softening, where the student mimics the probability distribution of the teacher, and intermediate-layer guidance, which aligns feature representations [13]. In multimodal domains, KD has enabled efficient training of smaller models for tasks involving text and vision, such as CLIP distillation [14]. Notably, KD has been explored in text-guided image generation and fusion, where computationally heavy models like Stable Diffusion serve as teachers for lightweight networks [15]. However, the distillation of semantic priors from LLMs and multimodal models in the domain of image fusion remains an open problem.

## 3 Method

### 3.1 Framework

Traditional image fusion methods formulate the task as mapping two source images (e.g.,  $\mathbf{I}_{\text{vis}}$ ,  $\mathbf{I}_{\text{ir}}$ ) to a fused output  $\mathbf{I}_{\text{f}}$  through a fusion network  $\Phi(\cdot)$ :

$$\mathbf{I}_{\text{f}} = \Phi(\mathbf{I}_{\text{vis}}, \mathbf{I}_{\text{ir}}) \quad (1)$$

Text-guided methods enhance this process by incorporating additional textual input, generated by large language models and encoded by CLIP to produce  $\mathbf{T}$ . The fused image  $\mathbf{I}_{\text{f}}$  is then generated using  $\mathbf{T}$  as guidance:

$$\mathbf{I}_{\text{f}} = \Phi(\mathbf{I}_{\text{vis}}, \mathbf{I}_{\text{ir}}, \mathbf{T}) \quad (2)$$

However, the computational cost of LLMs and CLIP is substantial. To mitigate this, we propose a prior distillation framework consisting of a text-guided teacher network  $\Phi_t$  and its distilled student network  $\Phi_s$ . During training,  $\Phi_t$  utilizes textual information from MLLMs, which is then transferred to  $\Phi_s$  through our tailored prior distillation loss. Since semantic information is encoded across both spatial and channel dimensions, we introduce spatial-channel cross fusion blocks within the network. As illustrated in Figure 2, this framework enables the student network to internalize textual information while significantly reducing model size. Both networks share similar structural blocks, with the student network being more compact.

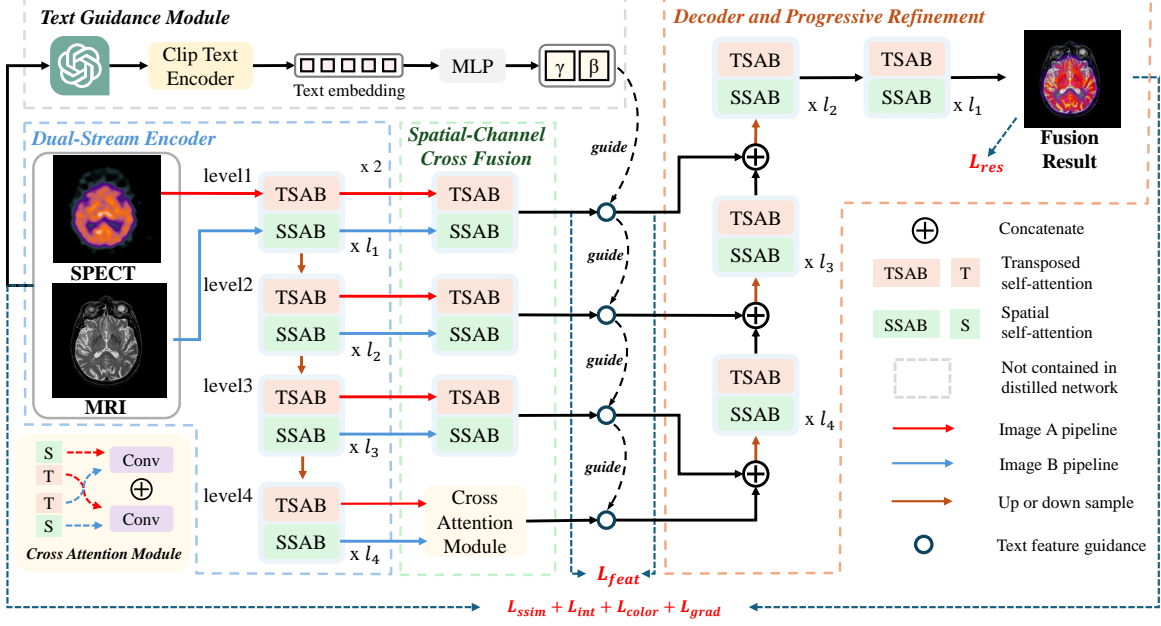


Figure 2: Overview of our text-guided image fusion framework. The architecture consists of three main components: (1) Text Guidance Module that leverages LLMs and CLIP to generate semantic guidance; (2) Encoder that processes visible and infrared inputs through dual-stream transformers with TSAB and SSAB blocks, followed by cross-modal fusion; (3) Decoder and Refinement that progressively reconstructs the fused image with text-guided feature modulation. Gray components are removed in the distilled student network. TSAB: Transposed Self-Attention Block, SSAB: Spatial Self-Attention Block.

## 3.2 Network Architecture

Our framework consists of two main components: a text-guided teacher network and a lightweight student network. The teacher network serves as a proxy, leveraging priors from the LLM and transferring this information to the student network in the form of features. The student network mimics the feature processing of the teacher, thus acquiring the semantic knowledge indirectly from the LLM. This enables the student network to maintain a small model size while being adaptive to image degradation, without requiring direct text input.

### 3.2.1 Text-Guided Teacher Network

The teacher network adopts a hierarchical structure with four levels of feature processing. Given its critical role in leveraging textual priors, the core operator aims to effectively modeling feature in spatial and channel dimensions [16]. Additionally, we introduce spatial-channel cross fusion blocks as the core operator, enabling the exploration of correlations between spatial and channel dimensions. Text information is fused through the sequential feature modulation, ensuring effective integration of textual priors. This network is organized into three primary components:

1) **Dual-Stream Encoder:** Dual-Stream Encoder: Processes visible and infrared inputs through parallel branches, each consisting of overlapped patch embedding layers and spatial and channel self-attention blocks. The hierarchical feature transformation at level  $l$  is expressed as:

$$F_l^i = \mathcal{F}_n \circ \mathcal{F}_{n-1} \circ \dots \circ \mathcal{F}_1(F_{l-1}^i) \quad (3)$$

where  $\mathcal{F}_k$  represents the  $k$ -th spatial-channel self-attention block for modality  $i \in vis, ir$ , and  $\circ$  denotes function composition. Each block integrates sequential Windowed Self-Attention Blocks (SSAB) and Transposed Self-Attention Blocks (TSAB) for comprehensive feature encoding:

$$\text{SSAB}(\mathbf{F}) = \mathbf{F} + \text{LN}(\text{MHA}_s(\mathbf{F})) \quad (4)$$

$$\text{TSAB}(\mathbf{F}) = \mathbf{F} + \text{LN}(\text{MHA}_c(\mathbf{F})) \quad (5)$$

Here,  $\text{MHA}_c(\cdot)$  and  $\text{MHA}_s(\cdot)$  denote multi-head attention mechanisms for channel and spatial dimensions [17, 18], respectively, and LN represents layer normalization.

2) **Spatial-Channel Cross Fusion:** To fully leverage prior information and establish the connection between two modalities, we propose the spatial-channel cross fusion module. At the upper level, features are concatenated and fused; at the lower level, features from both modalities are fused:

$$\mathbf{F}_l^{\hat{v}is} = \text{Conv1} \times 1 \circ C(\text{SSAB}(\mathbf{F}_l^{vis}), \text{TSAB}(\mathbf{F}_l^{ir})), \quad (6)$$

$$\mathbf{F}_l^{\hat{ir}} = \text{Conv1} \times 1 \circ C(\text{SSAB}(\mathbf{F}_l^{ir}), \text{TSAB}(\mathbf{F}_l^{vis})), \quad (7)$$

$$\mathbf{F}_l^{fused} = \mathbf{F}_l^{\hat{v}is} + \mathbf{F}_l^{\hat{ir}}. \quad (8)$$

where  $C(\cdot)$  denotes concatenation. The fused features are then modulated by the text embeddings:

$$\mathbf{F}_l^{\hat{fused}} = (1 + \gamma(\mathbf{T})) \odot \mathbf{F}_l^{fused} + \beta(\mathbf{T}) \quad (9)$$

where  $\gamma(\mathbf{T})$  and  $\beta(\mathbf{T})$  are learnable modulation parameters derived from the text embeddings  $\mathbf{T}$ , and  $\odot$  denotes element-wise multiplication.

3) **Decoder and Progressive Refinement:** The decoder progressively refines features through:

$$\mathbf{F}_{dec}^l = \mathcal{D}_n \circ \text{Up}(C(\mathbf{F}_{dec}^{l+1}, \mathbf{F}_{fused}^{\hat{l}})) \quad (10)$$

where  $\mathcal{D}_n$  represents a sequence of  $n$  decoder blocks similar to encoder. Specially, for the lowest level ( $l = 1$ ), we add extra decoder blocks as refinement:

$$\mathbf{F}_{out} = \mathcal{R}_m \circ \mathcal{R}_{m-1} \circ \dots \circ \mathcal{R}_1(\mathbf{F}_{dec}^1) \quad (11)$$

Each block  $\mathcal{R}_k$  consists of SSAB and TSAB operations shared block number with the encoder at corresponding level. At the end, the  $\mathbf{F}_{out}$  is the final result  $\mathbf{I}_{fused}$ .

### 3.2.2 Lightweight Student Network

The student network maintains a similar hierarchical structure but achieves 90% parameter reduction through:

1) Dimension reduction in transformer blocks (from 48 to 16 channels) 2) Removal of text guidance module, directly using  $\mathbf{F}_{fused}^l$  instead of  $\mathbf{F}_{fused}^{\hat{l}}$

### 3.3 Prior Knowledge Distillation

To achieve efficient inference without relying on MLLMs while preserving their semantic prior and reducing model complexity, we propose a two-stage knowledge distillation method to progressively transfer knowledge from MLLMs to a lightweight student network.

#### 3.3.1 Teacher Network Training

In the first stage, we transfer knowledge from the MLLM to a teacher network, enabling the teacher network to acquire semantic understanding and degradation-aware fusion capabilities. The teacher network is trained with text guidance using the following loss:

$$\mathcal{L}_{tea} = \lambda_s^t \mathcal{L}_{ssim} + \lambda_i^t \mathcal{L}_{int} + \lambda_g^t \mathcal{L}_{grad} + \lambda_c^t \mathcal{L}_{color} \quad (12)$$

where  $\mathcal{L}_{ssim}$  measures structural similarity through SSIM index,  $\mathcal{L}_{int}$  preserves maximum intensity information between source images,  $\mathcal{L}_{grad}$  ensures gradient consistency using Sobel operators, and  $\mathcal{L}_{color}$  maintains color fidelity in YCbCr space. The weights  $\lambda^t$  are dynamically adjusted based on text guidance. The details of these losses can be found in the supplementary material.

#### 3.3.2 Progressive Knowledge Transfer

In the second stage, the student network is trained to progressively acquire knowledge from the teacher network by mimicking its feature processing through three complementary loss functions:

1) Feature consistency loss:

$$\mathcal{L}_{feat} = \sum_{l=1}^L \|\text{Down}(F_t^l) - F_s^l\|_1 \quad (13)$$

where Down represents learnable dimension reduction to match teacher-student feature dimensions.

2) Output reconstruction loss:

$$\mathcal{L}_{res} = \|I_t^{fused} - I_s^{fused}\|_1 \quad (14)$$

3) Base fusion loss  $\mathcal{L}_{base}$  inherited from teacher but with fixed weights.

The final distillation objective is:

$$\mathcal{L}_{distill} = \alpha_1 \mathcal{L}_{base} + \alpha_2 \mathcal{L}_{feat} + \alpha_3 \mathcal{L}_{res} \quad (15)$$

This progressive distillation strategy enables knowledge transfer while reducing computational efficiency.

Table 1: Quantitative comparison with SOTA methods on IVF tasks. The number in () is non-trainable parameters but used in inference period. **Bold** and underlined values indicate the best and second-best results respectively. Params are measured in millions (M).

Method	Params(M)	MSRS			M3FD			RoadScene		
		EN $\uparrow$	VIF $\uparrow$	$Q^{AB/F} \uparrow$	EN $\uparrow$	VIF $\uparrow$	$Q^{AB/F} \uparrow$	EN $\uparrow$	VIF $\uparrow$	$Q^{AB/F} \uparrow$
SuperFusion	11.23	6.587	0.813	0.557	6.726	0.664	0.522	6.990	0.608	0.452
CDDFuse	2.40	6.701	0.819	0.548	<u>7.070</u>	0.802	0.613	<b>7.475</b>	0.610	0.450
IFCNN	0.08	5.975	0.579	0.479	<u>6.935</u>	0.685	0.590	7.222	0.591	0.536
U2Fusion	0.63	5.246	0.512	0.391	6.872	0.673	0.578	6.739	0.564	0.506
SwinFusion	13.04	6.619	0.825	0.558	6.844	0.746	0.616	7.000	0.614	0.450
PSLPT	3.06	6.307	0.753	0.553	<b>7.204</b>	<b>0.958</b>	0.321	7.077	0.134	0.171
TC-MOA	7.24(+329)	6.633	0.811	0.565	6.747	0.579	0.508	<u>7.387</u>	0.577	0.477
Text-IF	63.8(+151)	6.729	1.051	0.690	6.849	0.780	0.550	<u>7.332</u>	0.739	0.578
Ours-teacher	40.3(+151)	<u>6.749</u>	<u>1.060</u>	<u>0.732</u>	6.965	0.896	<b>0.706</b>	7.248	<u>0.743</u>	<b>0.639</b>
Ours-distilled	4.10	<b>6.763</b>	<b>1.075</b>	<b>0.734</b>	6.989	<u>0.927</u>	<u>0.704</u>	7.279	<b>0.751</b>	<u>0.634</u>

## 4 Experiments

We conduct extensive experiments to evaluate our proposed method on both infrared-visible fusion (IVF) and medical image fusion tasks. In this section, we first introduce the implementation details and datasets, then present comprehensive comparisons with state-of-the-art methods, followed by detailed ablation studies.

### 4.1 Implementation Details and Datasets

**Implementation Details:** Both teacher and student networks are trained using AdamW optimizer with a learning rate of 0.0001. Input images are cropped to  $128 \times 128$  patches during training. For the teacher network without text guidance, the hyper-parameters  $\{\lambda_i, \lambda_s, \lambda_g, \lambda_c\}$  are set to  $\{24, 40, 48, 12\}$  respectively. When text guidance is enabled, task-specific parameters are provided in the supplementary material. We employ QWen2VL [19], a open source large vision-language model, to generate descriptive text labels for input image pairs. All experiments are conducted on four NVIDIA GeForce RTX 4090 GPUs using PyTorch framework.

**Datasets:** For IVF tasks, we evaluate on three widely-used datasets: MSRS [20], M3FD [21], and RoadScene [22]. These datasets cover diverse scenarios including urban scenes, indoor environments, and road conditions with varying lighting and weather conditions. We use the training split of MSRS for training and evaluate on its test split as well as the entire M3FD and RoadScene datasets. For medical image fusion, we utilize the Harvard Medical Image Fusion Dataset, which contains three modality pairs: SPECT-MRI, CT-MRI, and PET-MRI. Each modality pair is trained and evaluated separately.

**Evaluation Metrics:** For IVF tasks, we employ three complementary metrics: Information Entropy (EN) [23] to quantify information density, Visual Information Fidelity (VIF) [24] to evaluate perceptual quality, and Quality of Gradient-based Fusion ( $Q^{AB/F}$ ) [25] to assess edge preservation. For medical image fusion, we include Structural

Similarity (SSIM) [26] due to its critical role in medical applications, which is calculated as the sum of the SSIM values between each source image and the fused image. The metrics are chosen for their strong correlation with the source images, as they take all of the images as input.

**Benchmark Methods:** We compare our teacher and distilled networks with several state-of-the-art methods, including SwinFusion [3], U2Fusion [2], CDDFuse [27], FusionGAN [1], PIAFusion [4], SuperFusion [28], IFCNN [29], DDFM [9], Text-IF [5], TC-MOA [30], PSLPT [31], EMFusion [32], Zero [30], and MSRPAN [31]. These methods include transformer-based, unsupervised learning, dual-branch, generative models, illumination- and semantic-aware fusion, CNN-based fusion, diffusion models, and text-guided fusion (Text-IF). Beyond performance comparisons, we focus on analyzing the impact of different components and parameters on both model effectiveness and inference efficiency through comprehensive ablation studies.

## 4.2 Comparison on IVF Tasks

Table 1 presents the quantitative comparison with SOTA methods on three IVF datasets. Our teacher network consistently outperforms existing methods across all metrics and datasets, demonstrating the effectiveness of text-guided fusion. On the MSRS dataset, our teacher network achieves significant improvements in  $Q^{AB/F}$  compared to the previous best method Text-IF. More remarkably, our distilled student network not only maintains but sometimes exceeds the

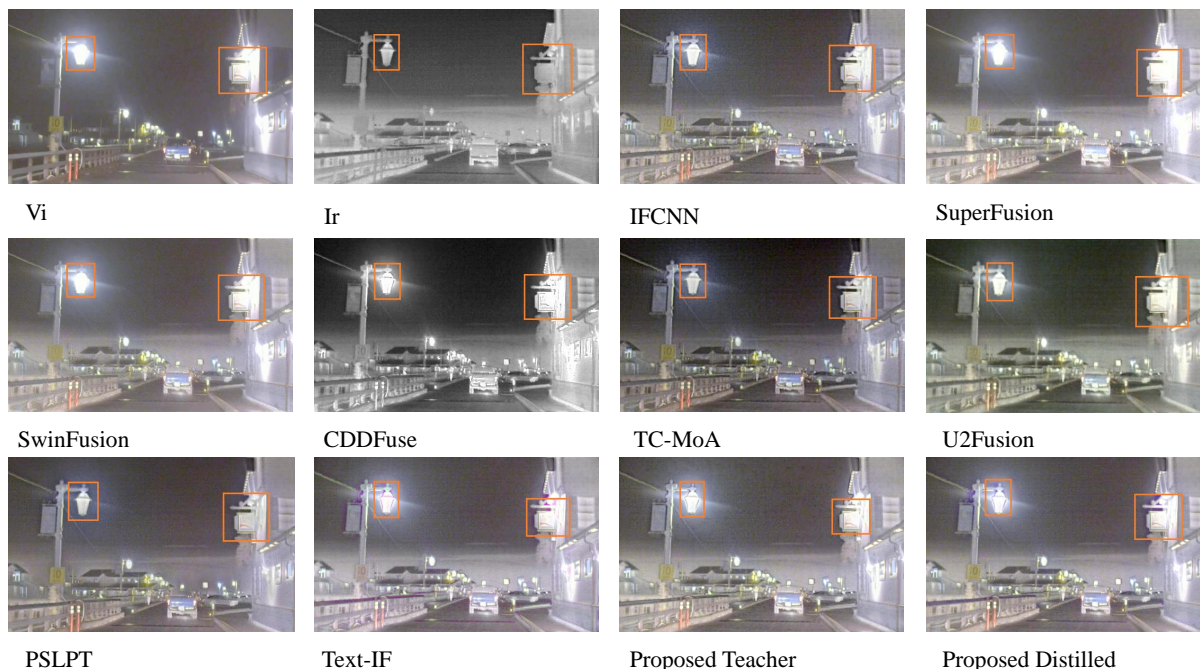


Figure 3: Compare with different methods on FLIR\_05767.jpg in RoadScene datasets. More can be found in appendix.

teacher’s performance, particularly in EN and  $Q^{AB/F}$  metrics, while reducing parameters by 90%. This suggests that the knowledge distillation process effectively transfers the teacher’s knowledge to a much smaller model. The slight performance variations between teacher and student networks can be attributed to the extended training during the distillation process, where the student benefits from both the teacher’s guidance and task-specific objectives. Another reason is that current domain models are generally over-parameterized compared to relatively small datasets, which is detailed in the ablation experiments. Figure 3 shows qualitative comparisons on challenging cases from different datasets. Our method better preserves thermal information from infrared images while maintaining visible details and natural appearance, especially in scenarios with extreme lighting conditions or complex textures.

## 4.3 Comparison on Medical Datasets

To demonstrate the generalization capability of our method, we evaluate its performance on medical image fusion tasks. As shown in Table 2, both our teacher and student networks achieve superior performance across different modality pairs. The improvement is particularly significant in structural preservation metrics (SSIM and  $Q^{AB/F}$ ),

Table 2: Quantitative comparison on Harvard Medical Dataset. The number in () is non-trainable parameters but used in inference period. **Bold** and underlined values indicate the best and second-best results respectively.

Method	Params(M)	PET-MRI			CT-MRI			SPECT-MRI		
		SSIM $\uparrow$	VIF $\uparrow$	$Q^{AB/F}\uparrow$	SSIM $\uparrow$	VIF $\uparrow$	$Q^{AB/F}\uparrow$	SSIM $\uparrow$	VIF $\uparrow$	$Q^{AB/F}\uparrow$
PSLPT	3.06	0.815	0.548	0.373	0.810	0.502	0.432	0.933	0.359	0.325
EMFusion	0.78	1.221	0.685	0.783	1.266	0.552	0.475	1.212	0.665	0.692
MSRPAN	0.39	1.182	0.581	<b>0.799</b>	1.261	0.436	0.455	1.153	0.525	0.560
SwinFusion	13.04	0.725	0.703	0.683	0.579	0.522	0.545	0.684	0.744	0.720
Zero	19.1	1.162	0.635	0.774	1.199	0.320	<u>0.582</u>	1.180	0.582	0.681
U2Fusion	0.63	0.494	0.460	0.292	0.042	0.074	0.489	0.479	0.419	0.696
CDDFuse	2.4	1.227	0.650	0.765	1.224	0.526	0.530	1.169	0.786	0.719
Text-IF	63.8(+151)	<u>1.232</u>	0.640	0.690	<b>1.313</b>	0.542	0.561	1.200	0.747	0.715
Ours-teacher	40.3(+151)	1.223	<u>0.909</u>	0.782	<b>1.313</b>	<u>0.641</u>	<b>0.657</b>	<b>1.210</b>	<b>0.888</b>	<u>0.746</u>
Ours-distilled	<b>4.1</b>	<b>1.243</b>	<b>0.929</b>	<u>0.784</u>	<u>1.312</u>	<b>0.653</b>	<b>0.657</b>	<u>1.202</u>	<u>0.887</u>	<b>0.747</b>

which is crucial for medical applications. For SPECT-MRI fusion, our method shows notable advantages in preserving

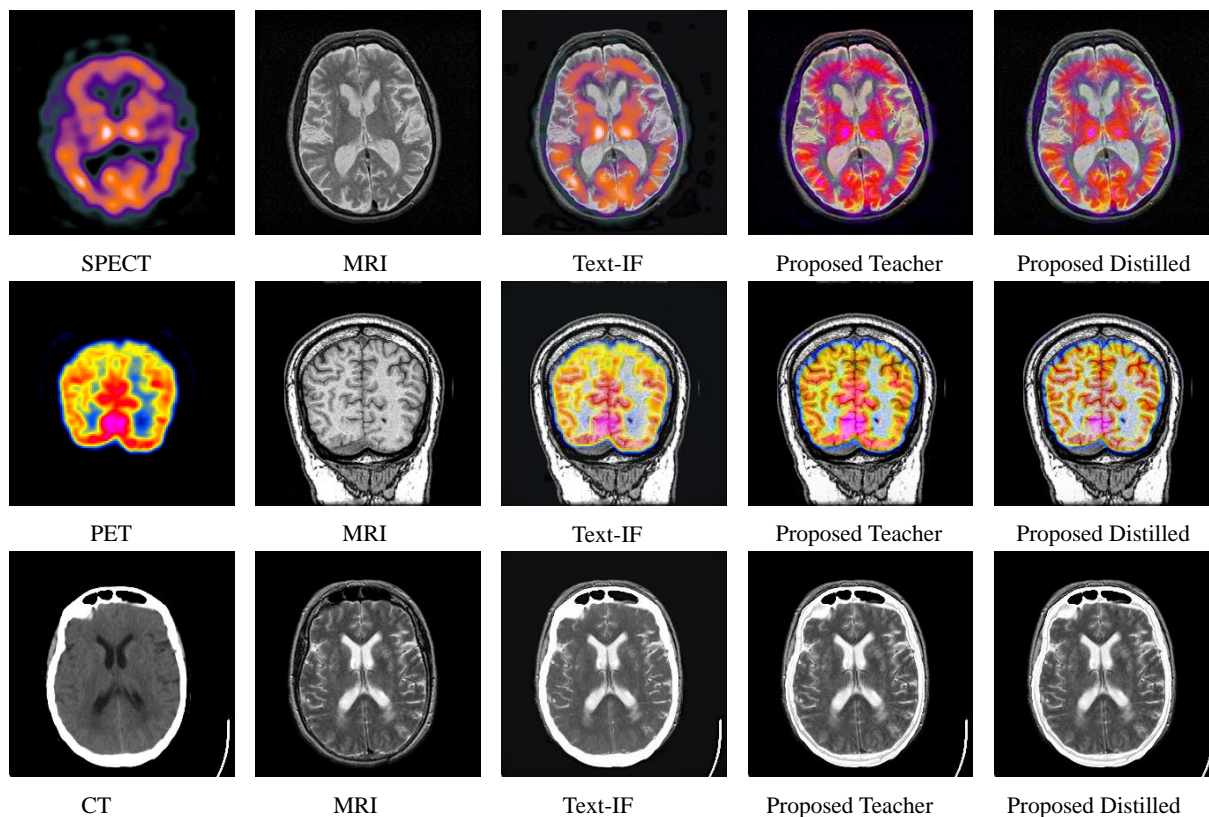


Figure 4: Compare with previous SOTA text-guided image fusion method Text-IF on Harvard Medical Image Fusion Datasets. More can be found in appendix.

functional information while maintaining anatomical details. In CT-MRI fusion, where structural alignment is critical, our approach achieves the highest SSIM scores, indicating better structural preservation. The PET-MRI results further confirm our method’s effectiveness in handling multi-modal medical images with different characteristics. Figure4 presents visual examples from different medical modalities. Our fusion results exhibit better detail preservation and contrast enhancement, which is essential for clinical applications. The distilled student network maintains these advantages while significantly reducing computational requirements, making it more practical for clinical deployment.

## 4.4 Ablation Study

To thoroughly evaluate the effectiveness of our proposed method, we conduct comprehensive ablation studies on both the teacher and student networks using the MSRS test set. These experiments examine the impact of text guidance, various loss components, and model architectures. Specifically, we address key questions such as: Why does the distilled network sometimes achieve a higher score than the teacher? Is it more effective to train a small model directly instead of using distillation?

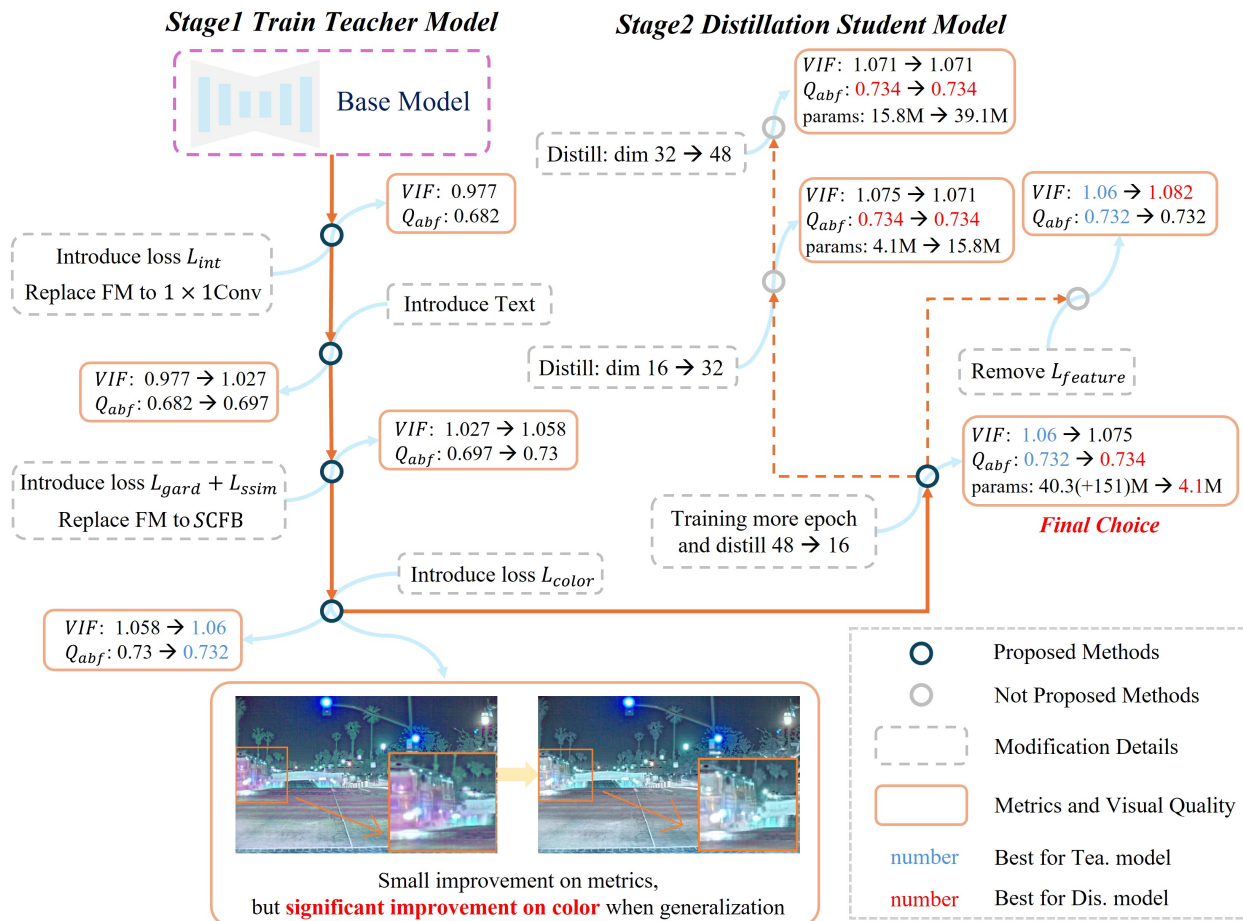


Figure 5: Overview of our ablation study

### 4.4.1 Analysis of Teacher Network

**Effect of Text Guidance.** To validate the effectiveness of text guidance, we compare our full model with its variant without text information. As shown in Table 3, removing text guidance leads to a significant performance drop across all metrics (EN: -0.023, VIF: -0.083,  $Q^{AB/F}$ : -0.05). This demonstrates that text descriptions provide valuable semantic information that helps the model better understand and fuse image features. This also demonstrates the effectiveness of our model distillation. The text guidance acts as an advanced form of reference information, offering rich contextual information beyond pixel-level features.

Table 3: Ablation study on text guidance. Results on MSRS test set.

Method	EN $\uparrow$	VIF $\uparrow$	$Q^{AB/F}$ $\uparrow$
Non-text	6.726	0.977	0.682
With text	<u>6.749</u>	<u>1.060</u>	<u>0.732</u>
Distilled	<b>6.763</b>	<b>1.075</b>	<b>0.734</b>

**Impact of Different Loss Components.** We evaluate the contribution of each loss component by systematically removing them from the full model. As shown in Table 4, all loss components positively impact the final performance, although their importance varies. The intensity loss ( $\mathcal{L}_{int}$ ) and gradient loss ( $\mathcal{L}_{grad}$ ) have the most significant influence, highlighting their essential role in preserving structural information. The SSIM loss ( $\mathcal{L}_{ssim}$ ) aids in maintaining perceptual quality, while the color loss ( $\mathcal{L}_{color}$ ) ensures the natural appearance of fused results.

Due to the nature of our method, which reconstructs the entire image rather than only modifying the Y-axis in YCbCr color space,  $\mathcal{L}_{color}$  plays a particularly important role. Although most metrics convert images to grayscale for evaluation, making  $\mathcal{L}_{color}$  appear to have minimal effect on metric scores, it is critical for producing visually appealing results in the final fused images.

Table 4: Ablation study on loss components for the teacher network. Results are reported on the MSRS test set.

Method	EN $\uparrow$	VIF $\uparrow$	$Q^{AB/F}$ $\uparrow$
$\mathcal{L}_{int}$	6.695	1.027	0.697
$\mathcal{L}_{int} + \mathcal{L}_{color}$	6.696	1.025	0.698
$\mathcal{L}_{int} + \mathcal{L}_{grad} + \mathcal{L}_{ssim}$	6.731	1.058	0.730
$\mathcal{L}_{int} + \mathcal{L}_{color} + \mathcal{L}_{grad}$	6.733	1.059	0.733
$\mathcal{L}_{color} + \mathcal{L}_{grad} + \mathcal{L}_{ssim}$	6.676	1.063	0.728
$\mathcal{L}_{color} + \mathcal{L}_{grad} + \mathcal{L}_{ssim} + \mathcal{L}_{int}$	<b>6.763</b>	<b>1.075</b>	<b>0.734</b>

**Feature Fusion Methods.** We investigate different fusion embedding strategies to combine features from infrared and visible images. The comparison includes concatenation, addition, and our proposed adaptive fusion method. Results demonstrate that our adaptive fusion approach achieves superior performance by dynamically adjusting the fusion weights based on spatial and channel features.

Table 5: Comparison of different fusion modules. Results on MSRS test set.

Method	EN $\uparrow$	VIF $\uparrow$	$Q^{AB/F}$ $\uparrow$
Cat & 1x1 conv	6.738	1.059	0.728
Unlearn weight atten	6.667	0.971	0.655
Dynamic weight conv	6.737	1.058	0.729
Multiscale conv	6.743	1.053	0.720
Ours	<b>6.749</b>	<b>1.060</b>	<b>0.732</b>

#### 4.4.2 Analysis of Student Network

**Effect of Model Size.** A notable finding in our distillation experiments is that reducing the model size by up to 90% (from 40.3M to 4.1M parameters if not calculate CLIP) does not significantly impact performance. As shown in Table 6, the compact student model maintains comparable or even slightly better results across different metrics. This suggests that the original model might be over-parameterized for the current fusion task, and the knowledge distillation process effectively transfers essential fusion capabilities to a much smaller architecture.

Table 6: Impact of model size on distilled network. Results on MSRS test set.

Model	Params(M)	EN $\uparrow$	VIF $\uparrow$	$Q^{AB/F}$ $\uparrow$
48dim	39.1	<b>6.780</b>	1.071	<b>0.734</b>
32dim	15.8	6.768	1.071	<b>0.734</b>
16dim	<b>4.1</b>	6.763	<b>1.075</b>	<b>0.734</b>

**Impact of Distillation Losses.** We evaluate the contribution of different components in our distillation framework. The results in Table 7 show that result-level supervision (matching the teacher’s output) provides strong guidance, significantly improving the student model’s performance. The feature distillation loss, on the other hand, plays a key role in preserving feature-level consistency, ensuring that the student model captures important intermediate representations from the teacher. By introducing feature distillation, the model learns high-frequency details and intermediate features,

enriching the information. This improves metrics like  $EN$  and  $Q^{AB/F}$ , though it may slightly reduce the  $VIF$  score due to imperfect alignment with perceptual fidelity.

Table 7: Ablation study on distillation losses (MSRS dataset).

Method	EN $\uparrow$	VIF $\uparrow$	$Q^{AB/F}$ $\uparrow$
$\mathcal{L}_{base}$	6.728	0.989	0.681
$\mathcal{L}_{base} + \mathcal{L}_{res}$	6.761	<b>1.082</b>	<u>0.732</u>
$\mathcal{L}_{base} + \mathcal{L}_{feat} + \mathcal{L}_{res}$	<b>6.763</b>	<u>1.075</u>	<b>0.734</b>

Our ablation studies reveal several key insights:

- Text guidance significantly enhances fusion performance by embedding rich semantic context into the process.
- The integration of multiple loss terms is crucial for achieving balanced and robust fusion results.
- Model compression via knowledge distillation achieves comparable performance with drastically fewer parameters, as the teacher model and some text-guided methods exhibit excessive over-parameterization compared to small datasets.

## 5 Conclusion

We address the weak semantic understanding of traditional image fusion methods and the high cost of text-guided approaches by distilling textual priors and eliminating the need for text guidance during inference. Our approach, which leverages a teacher-student architecture and tailored prior distillation, significantly reduces the model size while retaining high performance. Extensive experiments and ablation studies validate the effectiveness of our method, highlighting its ability to achieve a strong trade-off between computational efficiency and fusion quality. We also analyze the contribution of individual components, offering valuable insights into their roles in the overall performance. Interestingly, we observe that the distilled model occasionally outperforms the teacher model, a phenomenon we discuss further in the appendix.

## References

- [1] Jiayi Ma, Wei Yu, Pengwei Liang, Chang Li, and Junjun Jiang. Fusiongan: A generative adversarial network for infrared and visible image fusion. *Information Fusion*, 48:11–26, 2019.
- [2] Han Xu, Jiayi Ma, Junjun Jiang, Xiaojie Guo, and Haibin Ling. U2fusion: A unified unsupervised image fusion network. *IEEE Transactions on Pattern Analysis and Machine Intelligence*, 44(1):502–518, 2020.
- [3] Jiayi Ma, Linfeng Tang, Fan Fan, Jun Huang, Xiaoguang Mei, and Yong Ma. Swinfusion: Cross-domain long-range learning for general image fusion via swin transformer. *IEEE/CAA Journal of Automatica Sinica*, 9(7):1200–1217, 2022.
- [4] Linfeng Tang, Jiteng Yuan, Hao Zhang, Xingyu Jiang, and Jiayi Ma. Piafusion: A progressive infrared and visible image fusion network based on illumination aware. *Information Fusion*, 83-84:79–92, 2022.
- [5] Xunpeng Yi, Han Xu, Hao Zhang, Linfeng Tang, and Jiayi Ma. Text-if: Leveraging semantic text guidance for degradation-aware and interactive image fusion. In *Proceedings of the IEEE/CVF Conference on Computer Vision and Pattern Recognition (CVPR)*, 2024.
- [6] Jinze Bai, Shuai Bai, Shusheng Yang, Shijie Wang, Sinan Tan, Peng Wang, Junyang Lin, Chang Zhou, and Jingren Zhou. Qwen-vl: A versatile vision-language model for understanding, localization, text reading, and beyond. *arXiv preprint arXiv:2308.12966*, 2023.
- [7] Alec Radford, Jong Wook Kim, Chris Hallacy, Aditya Ramesh, Gabriel Goh, Sandhini Agarwal, Girish Sastry, Amanda Askell, Pamela Mishkin, Jack Clark, Gretchen Krueger, and Ilya Sutskever. Learning transferable visual models from natural language supervision. *CoRR*, abs/2103.00020, 2021.
- [8] Chunyang Cheng, Tianyang Xu, Xiao-Jun Wu, Hui Li, Xi Li, Zhangyong Tang, and Josef Kittler. Textfusion: Unveiling the power of textual semantics for controllable image fusion. *arXiv preprint arXiv:2312.14209*, 2023.
- [9] Zixiang Zhao, Haowen Bai, Yuanzhi Zhu, Jianshe Zhang, Shuang Xu, Yulun Zhang, Kai Zhang, Deyu Meng, Radu Timofte, and Luc Van Gool. Ddfm: Denoising diffusion model for multi-modality image fusion. In *Proceedings of the IEEE/CVF International Conference on Computer Vision (ICCV)*, pages 8082–8093, October 2023.

- [10] Man Zhou, Naishan Zheng, Xuanhua He, Danfeng Hong, and Jocelyn Chanussot. Probing synergistic high-order interaction for multi-modal image fusion. *IEEE Transactions on Pattern Analysis and Machine Intelligence*, 2024.
- [11] Bing Cao, Yiming Sun, Pengfei Zhu, and Qinghua Hu. Multi-modal gated mixture of local-to-global experts for dynamic image fusion. In *Proceedings of the IEEE/CVF International Conference on Computer Vision*, pages 23555–23564, 2023.
- [12] Geoffrey Hinton. Distilling the knowledge in a neural network. *arXiv preprint arXiv:1503.02531*, 2015.
- [13] Li Yuan, Francis EH Tay, Guilin Li, Tao Wang, and Jiashi Feng. Revisiting knowledge distillation via label smoothing regularization. In *Proceedings of the IEEE/CVF conference on computer vision and pattern recognition*, pages 3903–3911, 2020.
- [14] Kan Wu, Houwen Peng, Zhenghong Zhou, Bin Xiao, Mengchen Liu, Lu Yuan, Hong Xuan, Michael Valenzuela, Xi Stephen Chen, Xinggong Wang, et al. Tinyclip: Clip distillation via affinity mimicking and weight inheritance. In *Proceedings of the IEEE/CVF International Conference on Computer Vision*, pages 21970–21980, 2023.
- [15] Yang Zhao, Yanwu Xu, Zhisheng Xiao, and Tingbo Hou. Mobilediffusion: Subsecond text-to-image generation on mobile devices. *arXiv preprint arXiv:2311.16567*, 2023.
- [16] Xiangyu Chen, Zheyuan Li, Yuandong Pu, Yihao Liu, Jiantao Zhou, Yu Qiao, and Chao Dong. A comparative study of image restoration networks for general backbone network design. In *European Conference on Computer Vision*, pages 74–91. Springer, 2025.
- [17] Syed Waqas Zamir, Aditya Arora, Salman Khan, Munawar Hayat, Fahad Shahbaz Khan, and Ming-Hsuan Yang. Restormer: Efficient transformer for high-resolution image restoration. In *CVPR*, 2022.
- [18] Ze Liu, Yutong Lin, Yue Cao, Han Hu, Yixuan Wei, Zheng Zhang, Stephen Lin, and Baining Guo. Swin transformer: Hierarchical vision transformer using shifted windows. In *Proceedings of the IEEE/CVF international conference on computer vision*, pages 10012–10022, 2021.
- [19] Peng Wang, Shuai Bai, Sinan Tan, Shijie Wang, Zhihao Fan, Jinze Bai, Keqin Chen, Xuejing Liu, Jialin Wang, Wenbin Ge, Yang Fan, Kai Dang, Mengfei Du, Xuancheng Ren, Rui Men, Dayiheng Liu, Chang Zhou, Jingren Zhou, and Junyang Lin. Qwen2-vl: Enhancing vision-language model’s perception of the world at any resolution. *arXiv preprint arXiv:2409.12191*, 2024.
- [20] Linfeng Tang, Jiteng Yuan, Hao Zhang, Xingyu Jiang, and Jiayi Ma. MSRS: Multi-Spectral Road Scenarios for Practical Infrared and Visible Image Fusion. <https://github.com/Linfeng-Tang/MSRS>, 2022.
- [21] Jinyuan Liu, Xin Fan, Zhanbo Huang, Guanyao Wu, Risheng Liu, Wei Zhong, and Zhongxuan Luo. Target-aware dual adversarial learning and a multi-scenario multi-modality benchmark to fuse infrared and visible for object detection. In *Proceedings of the IEEE/CVF Conference on Computer Vision and Pattern Recognition*, pages 5802–5811, 2022.
- [22] Han Xu, Jiayi Ma, Zhuliang Le, Junjun Jiang, and Xiaojie Guo. Fusiondn: A unified densely connected network for image fusion. In *proceedings of the Thirty-Fourth AAAI Conference on Artificial Intelligence*, 2020.
- [23] J. Wesley Roberts, Jan A. van Aardt, and Fethi Babikker Ahmed. Assessment of image fusion procedures using entropy, image quality, and multispectral classification. *Journal of Applied Remote Sensing*, 2(1):023522, 2008.
- [24] Yu Han, Yunze Cai, Yin Cao, and Xiaoming Xu. A new image fusion performance metric based on visual information fidelity. *Information Fusion*, 14(2):127–135, 2013.
- [25] G. Piella and H. Heijmans. A new quality metric for image fusion. In *Proceedings 2003 International Conference on Image Processing (Cat. No.03CH37429)*, volume 3, pages III–173, 2003.
- [26] Zhou Wang, A.C. Bovik, H.R. Sheikh, and E.P. Simoncelli. Image quality assessment: from error visibility to structural similarity. *IEEE Transactions on Image Processing*, 13(4):600–612, 2004.
- [27] Zixiang Zhao, Haowen Bai, Jianshe Zhang, Yulun Zhang, Shuang Xu, Zudi Lin, Radu Timofte, and Luc Van Gool. Cddfuse: Correlation-driven dual-branch feature decomposition for multi-modality image fusion. In *Proceedings of the IEEE/CVF conference on computer vision and pattern recognition*, pages 5906–5916, 2023.
- [28] Linfeng Tang, Yuxin Deng, Yong Ma, Jun Huang, and Jiayi Ma. Superfusion: A versatile image registration and fusion network with semantic awareness. *IEEE/CAA Journal of Automatica Sinica*, 9(12):2121–2137, 2022.
- [29] Yu Zhang, Yu Liu, Peng Sun, Han Yan, Xiaolin Zhao, and Li Zhang. Ifcnn: A general image fusion framework based on convolutional neural network. *Information Fusion*, 54:99–118, 2020.
- [30] Pengfei Zhu, Yang Sun, Bing Cao, and Qinghua Hu. Task-customized mixture of adapters for general image fusion. In *Proceedings of the IEEE/CVF Conference on Computer Vision and Pattern Recognition*, 2024.

- [31] Wu Wang, Liang-Jian Deng, and Gemine Vivone. A general image fusion framework using multi-task semi-supervised learning. *Information Fusion*, page 102414, 2024.
- [32] Han Xu and Jiayi Ma. Emfusion: An unsupervised enhanced medical image fusion network. *Information Fusion*, 2021.
- [33] Xiangyu Chen, Zheyuan Li, Yuandong Pu, Yihao Liu, Jiantao Zhou, Yu Qiao, and Chao Dong. A comparative study of image restoration networks for general backbone network design, 2024.
- [34] Or Patashnik, Zongze Wu, Eli Shechtman, Daniel Cohen-Or, and Dani Lischinski. Styleclip: Text-driven manipulation of stylegan imagery. *CoRR*, abs/2103.17249, 2021.
- [35] Robin Rombach, Andreas Blattmann, Dominik Lorenz, Patrick Esser, and Björn Ommer. High-resolution image synthesis with latent diffusion models, 2021.
- [36] V. Petrovic and C. Xydeas. Objective image fusion performance characterisation. In *Tenth IEEE International Conference on Computer Vision (ICCV'05) Volume 1*, volume 2, pages 1866–1871 Vol. 2, 2005.
- [37] Xiao Xiang Zhu and Richard Bamler. A sparse image fusion algorithm with application to pan-sharpening. *IEEE Transactions on Geoscience and Remote Sensing*, 51(5):2827–2836, 2013.
- [38] Jun Fu, Weisheng Li, Jiao Du, and Yuping Huang. A multiscale residual pyramid attention network for medical image fusion. *Biomedical Signal Processing and Control*, 66:102488, 2021.
- [39] Fayez Lahoud and Sabine Süssstrunk. Zero-learning fast medical image fusion. In *2019 22th International Conference on Information Fusion (FUSION)*, pages 1–8, 2019.
- [40] Dan Guo, Kun Li, Bin Hu, Yan Zhang, and Meng Wang. Benchmarking micro-action recognition: Dataset, methods, and applications. *IEEE Transactions on Circuits and Systems for Video Technology*, 34(7):6238–6252, 2024.
- [41] Hessah Albarqaan, Rongjun Qin, and Yang Teng. Image Fusion in Remote Sensing: An Overview and Meta-Analysis. *Photogrammetric Engineering & Remote Sensing*, 90(12):755–775, December 2024.
- [42] Jiayi Ma, Yong Ma, and Chang Li. Infrared and visible image fusion methods and applications: A survey. *Information Fusion*, 45:153–178, 2019.
- [43] Tri Dao, Daniel Y. Fu, Stefano Ermon, Atri Rudra, and Christopher Ré. FlashAttention: Fast and memory-efficient exact attention with IO-awareness. In *Advances in Neural Information Processing Systems (NeurIPS)*, 2022.
- [44] Tri Dao. FlashAttention-2: Faster attention with better parallelism and work partitioning. In *International Conference on Learning Representations (ICLR)*, 2024.

## A Teacher Network Loss Terms

This section will introduce complete mathematical formulations for all loss terms which we used in the train process of teacher network.

$$\mathcal{L}_{tea} = \lambda_{ssim}^t \mathcal{L}_{ssim} + \lambda_{int}^t \mathcal{L}_{int} + \lambda_{grad}^t \mathcal{L}_{grad} + \lambda_{color}^t \mathcal{L}_{color} \quad (16)$$

where  $\mathcal{L}_{ssim}$  measures structural similarity through SSIM index,  $\mathcal{L}_{int}$  preserves maximum intensity information between source images,  $\mathcal{L}_{grad}$  ensures gradient consistency using Sobel operators, and  $\mathcal{L}_{color}$  maintains color fidelity in YCbCr space. The weights  $\lambda^t$  are dynamically adjusted based on text guidance. The detailed expressions for each loss component are:

$$\mathcal{L}_{int} = \frac{1}{HW} \|I_f - \max(I_{vis}^g, I_{ir}^g)\|_1 \quad (17)$$

where  $H$  and  $W$  are the height and width of the image,  $I_f$  is the fused image, and  $I_{vis}^g$  and  $I_{ir}^g$  represent the visible and infrared guidance images respectively.

$$\mathcal{L}_{SSIM}(t) = (1 - SSIM(I_f, I_{vis}^g)) + \delta_{ir}(t)(1 - SSIM(I_f, I_{ir}^g)) \quad (18)$$

where  $SSIM(\cdot)$  calculates the structural similarity index, and  $\delta_{ir}(t)$  is a text-dependent weight for infrared guidance.

$$\mathcal{L}_{grad} = \frac{1}{HW} \|\nabla I_f - \max(\nabla I_{vis}^g, \nabla I_{ir}^g)\|_1 \quad (19)$$

where  $\nabla$  represents the gradient operator implemented using Sobel filters in both horizontal and vertical directions.

$$\mathcal{L}_{color} = \frac{1}{HW} \|F_{CbCr}(I_f) - F_{CbCr}(I_{vis}^g)\|_1 \quad (20)$$

where  $F_{CbCr}$  denotes the transfer function of RGB to YCbCr.

These loss terms work together to ensure high-quality image fusion:  $\mathcal{L}_{int}$  maintains the maximum intensity information from both source images,  $\mathcal{L}_{SSIM}$  preserves structural details through the SSIM[26] metric,  $\mathcal{L}_{grad}$  ensures edge consistency through gradient preservation, and  $\mathcal{L}_{color}$  maintains natural color appearance. The text-dependent weights  $\alpha(t)$  allow dynamic adjustment of each loss component’s contribution based on the specific fusion requirements described in the text prompt.

## B Additional Quantitative Results

### B.1 More Comparison on Infrared-Visible Tasks

Due to space limitations in the main paper, we present additional evaluation metrics here. Table 10 provides a comprehensive comparison across three datasets (MSRS, M3FD, and RoadScene) using five metrics: Entropy (EN[23]), Mutual Information (MI[42]), Spatial Frequency (SF[36]), Visual Information Fidelity (VIF[24]), and Quality of Gradient-based Fusion ( $Q^{AB/F}$ ). Our method demonstrates consistent superiority across most metrics, particularly in structural preservation (VIF,  $Q^{AB/F}$ [25]) and information content (EN, MI).

The distilled student network achieves comparable or even better performance than the teacher network while using only 4.1M parameters, compared to the teacher’s 40.3M (+151M fixed parameters). This significant reduction in model size (approximately 90%) without performance degradation validates the effectiveness of our knowledge distillation approach. Notably, on the MSRS dataset, our distilled model improves upon the teacher network across all metrics, suggesting that the distillation process not only transfers knowledge but also helps regularize the model.

### B.2 More Comparison on Medical Images

Table 11 extends our evaluation to medical image fusion tasks across three modality pairs (PET-MRI, CT-MRI, and SPECT-MRI) using additional metrics including SSIM, VIF,  $Q^{AB/F}$ , MI, and EN. The results demonstrate our method’s strong generalization capability across different medical imaging modalities.

For PET-MRI fusion, our distilled model achieves the highest scores in SSIM (1.243) and VIF (0.929), indicating superior structural preservation and perceptual quality. In CT-MRI fusion, both teacher and student networks maintain high performance, particularly in structural metrics (SSIM: 1.313) and edge preservation ( $Q^{AB/F}$ : 0.657). The SPECT-MRI results further validate our method’s effectiveness, with the distilled network showing exceptional performance in information preservation (MI: 4.371) while maintaining high structural fidelity.

## C Extended qualitative Results

### C.1 Visual Comparison on Infrared-Visible Images

Figure 8 presents additional visual comparisons across different challenging scenarios from the MSRS, M3FD, and RoadScene datasets. Our method demonstrates superior performance in: 1) Preserving thermal information from infrared images while maintaining natural visible details 2) Handling extreme lighting conditions and complex textures 3) Maintaining clear object boundaries and structural integrity 4) Achieving balanced fusion results without introducing artifacts

### C.2 Visual Comparison on Medical Images

Figure 9 showcases detailed visual comparisons across different medical imaging modalities. The results highlight our method’s advantages in: 1) Preserving fine anatomical structures from both modalities 2) Maintaining clear tissue boundaries and contrast 3) Effectively combining functional information (PET/SPECT) with anatomical details (MRI) 4) Producing clinically meaningful fusion results with enhanced diagnostic value

## D Extend Ablation Studies

### D.1 Text Prior Analysis

To better understand how textual priors influence the fusion process, we conduct a detailed analysis of their effects at different network levels. As shown in Figure 6, we visualize the feature maps before and after applying text guidance, as well as the final fused results under different text descriptions.

The visualization reveals that text guidance significantly impacts the model’s attention to different image regions. For instance, when processing a low-contrast nighttime scene, the text prior helps the model better distinguish the vehicle’s contours from the background. This is evident in the feature maps, where the “After prompt guidance” visualization shows more defined object boundaries and clearer separation between foreground and background elements compared to the “Before prompt guidance” state.

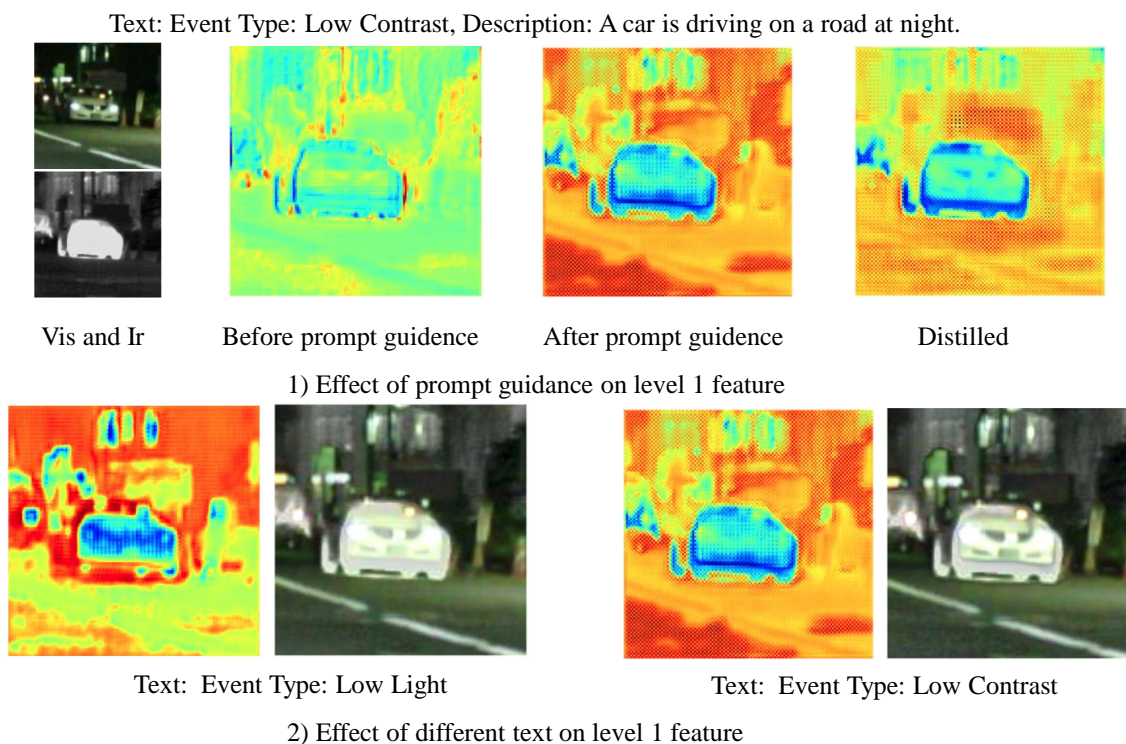


Figure 6: Effect of text guidance on level 1 and fused image.

Interestingly, different text descriptions (e.g., “Low Contrast” vs. “Low Light”) lead to distinct feature emphasis patterns. Under the “Low Light” condition, the model pays more attention to illumination-related features, while the “Low Contrast” description prompts the model to focus more on edge and boundary information. This demonstrates the model’s ability to adapt its fusion strategy based on the provided textual context.

The “Distilled” results show that our student network successfully inherits these text-guided attention patterns without requiring explicit textual input during inference. This validates the effectiveness of our prior distillation approach in preserving the semantic understanding capabilities of the teacher network while significantly reducing computational overhead.

## D.2 Knowledge Distillation Analysis

An intriguing observation from our experiments is that the distilled student network occasionally outperforms its teacher model. To investigate this phenomenon, we conducted a detailed analysis of the distillation process and its impact on model behavior.

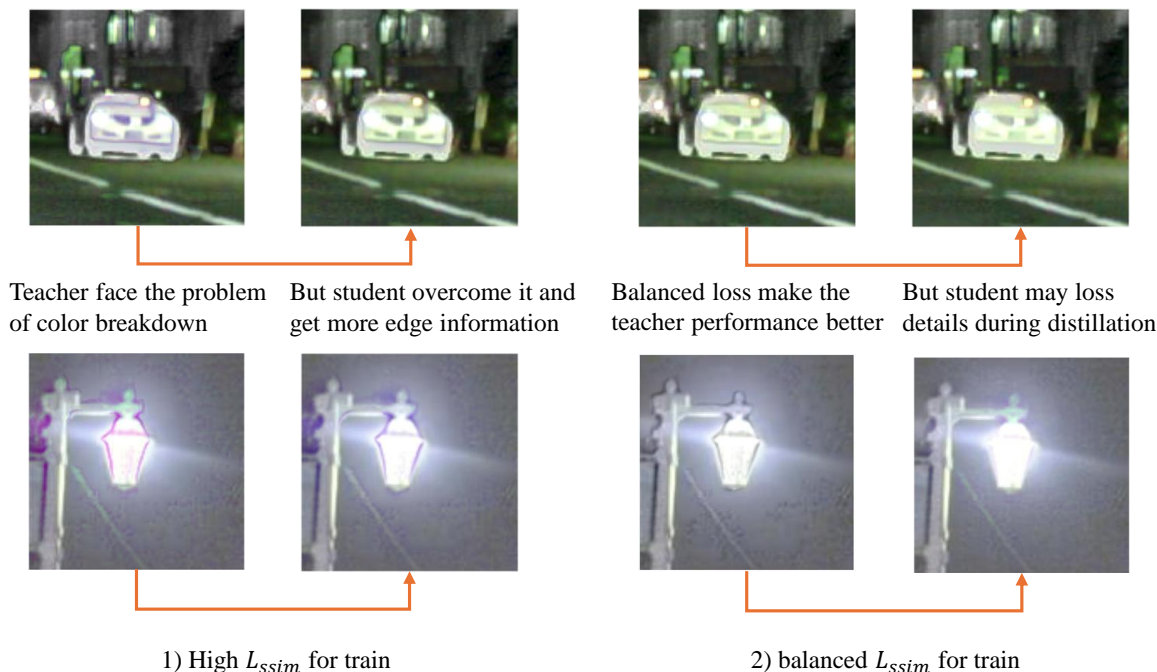


Figure 7: When teacher perform extremely, the student learn more information.

**Balance Between Structural and Color Information.** When training the teacher network with text guidance, we observed that increasing the weight of  $\mathcal{L}_{ssim}$  leads to stronger edge and boundary preservation but may cause color degradation issues. Interestingly, during the distillation process, the student network appears to naturally balance these competing objectives. As shown in Figure 7, while the teacher model might exhibit color breakdown when heavily prioritizing structural information, the student network maintains edge clarity while simultaneously preserving natural color representation.

**Impact of Teacher’s Behavior on Student Performance.** Our experiments reveal that the relationship between teacher and student performance is not strictly monotonic. We tested this by training teacher models with varying degrees of  $\mathcal{L}_{ssim}$  emphasis. With an extreme weighting (10× the baseline), the teacher model becomes highly specialized in edge detection but sacrifices other aspects of image quality. Surprisingly, this extreme specialization enables the student to learn more comprehensive fusion strategies, potentially due to the clearer supervision signal for structural features.

However, such extreme settings are primarily valuable for experimental analysis rather than practical applications. In our final implementation, we adopt a moderately increased weight for  $\mathcal{L}_{ssim}$  compared to our balanced version (where all loss components have equal weights). This moderate adjustment proves sufficient for the student network to achieve superior performance across multiple metrics while maintaining stable training dynamics.

This phenomenon might be attributed to several factors:

- The distillation process acts as a form of regularization, preventing the student from inheriting potential overfitting behaviors from the teacher
- The student network’s architecture may be better suited for balancing multiple objectives simultaneously

- The knowledge distillation framework allows the student to learn from the teacher’s intermediate representations, potentially capturing complementary information that aids in overall fusion quality

### D.3 Inference Time Analysis

To evaluate the computational efficiency, we analyze the inference times of different components across the previous state-of-the-art (SoTA) text-guided method Text-IF, our teacher network, and the distilled student network. For text generation, we use Qwen2-VL as the large language model (LLM), which operates on two NVIDIA RTX 4090 GPUs with the fast attention library[44]. Other timing experiments were conducted on a separate single NVIDIA RTX 4090 GPU, running with a batch size of 1 and an image resolution of  $128 \times 128$  pixels. Since these results may vary across different machines or even different states of the same machine, this comparison should be considered non-rigorous.

Table 8: Detailed inference time comparison (in milliseconds) for different components. LLM refers to the Qwen2-VL model used for text generation.

Method	Data Load	LLM	CLIP	Fusion	Total
Text-IF	0.01	2261.2	115.7	152.1	2529.01
Teacher	0.01	2311.1	112.4	133.4	2556.91
Student	0.01	-	-	<b>46.1</b>	46.11

As shown in Table 8, the LLM component dominates the computational cost, requiring over 2 seconds per image. CLIP encoding adds another 110-115ms overhead. While the teacher network’s fusion module takes 133.4ms, our distilled student network reduces this to just 46.1ms - a 65% reduction in fusion time. More importantly, by eliminating the need for LLM and CLIP during inference, our student network achieves a dramatic 98% reduction in total inference time (from 2556.91ms to 46.11ms).

### D.4 Limitations

While our distilled model achieves significant inference-time efficiency, we acknowledge a limitation in training overhead. The knowledge distillation process introduces additional computational costs during the training phase.

Table 9: Training time comparison for different epochs. All experiments were conducted on a single NVIDIA 4090 GPU.

Method	100 epochs	500 epochs
Text-IF	1.9h	11.1h
Teacher	2.0h	12.1h
Student (distill)	2.1h	13.5h

As shown in Table 9, our distillation approach requires slightly longer training time compared to both the baseline Text-IF and the teacher model. For a 100-epoch training cycle, the student network’s distillation process takes 2.1 hours, approximately 10.5% longer than Text-IF (1.9h) and 5% longer than the teacher model (2.0h). This pattern persists for longer training durations, with 500-epoch training requiring 13.5 hours for distillation compared to 11.1 hours for Text-IF and 12.1 hours for the teacher model.

This increased training time is primarily attributed to two factors: (1) the two-stage training process where the teacher must be trained first, and (2) the additional computational overhead from the distillation loss calculations. However, we consider this a reasonable trade-off given the substantial inference-time benefits, as the training process is typically a one-time cost while inference efficiency directly impacts real-world applications.



Figure 8: More compare with different methods on different datasets.

Table 10: Quantitative comparison with SOTA methods on IVF tasks. **Bold** and underlined values indicate the best and second-best results respectively. Tra.P. = Trainable Parameters, Fix.P. = Fixed Parameters

Dataset	Method	Tra.P. (M)	Fix.P. (M)	EN $\uparrow$	MI $\uparrow$	SF $\uparrow$	VIF $\uparrow$	$Q^{AB/F} \uparrow$
MSRS	SuperFusion[28]	11.23	-	6.587	3.596	10.783	0.813	0.557
	CDDFuse[27]	2.40	-	6.701	3.657	12.083	0.819	0.548
	IFCNN[29]	0.08	-	5.975	1.706	12.734	0.579	0.479
	U2Fusion[2]	0.63	-	5.246	2.183	9.242	0.512	0.391
	SwinFusion[3]	13.04	-	6.619	3.652	11.038	0.825	0.558
	PSLPT[31]	3.06	-	6.307	2.284	10.419	0.753	0.553
	TC-MOA[30]	7.24	(+329)	6.633	3.251	9.370	0.811	0.565
	Text-IF[5]	63.8	(+151)	6.729	<b>5.406</b>	17.384	1.051	0.690
	Ours-teacher	40.3	(+151)	<u>6.749</u>	<u>4.883</u>	<u>17.914</u>	<u>1.060</u>	<u>0.732</u>
	Ours-distilled	4.10	-	<b>6.763</b>	4.867	<b>18.299</b>	<b>1.075</b>	<b>0.734</b>
M3FD	SuperFusion[28]	11.23	-	6.726	4.345	11.748	0.664	0.522
	CDDFuse[27]	2.40	-	<u>7.070</u>	3.994	17.578	0.802	0.613
	IFCNN[29]	0.08	-	6.935	2.630	16.250	0.685	0.590
	U2Fusion[2]	0.63	-	6.872	2.683	14.248	0.673	0.578
	SwinFusion[3]	13.04	-	6.844	4.020	14.415	0.746	0.616
	PSLPT[31]	3.06	-	<b>7.204</b>	4.563	6.439	<b>0.958</b>	0.321
	TC-MOA[30]	7.24	(+329)	6.747	2.856	11.221	0.579	0.508
	Text-IF[5]	63.8	(+151)	6.849	<b>5.553</b>	14.484	0.780	0.550
	Ours-teacher	40.3	(+151)	6.965	4.780	<u>17.949</u>	0.896	<b>0.706</b>
	Ours-distilled	4.10	-	6.989	<u>4.898</u>	<b>18.507</b>	<u>0.927</u>	<u>0.704</u>
RoadScene	SuperFusion[28]	11.23	-	6.990	<u>3.562</u>	12.185	0.608	0.452
	CDDFuse[27]	2.40	-	<b>7.475</b>	3.001	19.779	0.610	0.450
	IFCNN[29]	0.08	-	7.222	2.842	15.998	0.591	0.536
	U2Fusion[2]	0.63	-	6.739	2.578	15.282	0.564	0.506
	SwinFusion[3]	13.04	-	7.000	3.334	12.161	0.614	0.450
	PSLPT[31]	3.06	-	7.077	2.001	9.172	0.134	0.171
	TC-MOA[30]	7.24	(+329)	<u>7.387</u>	2.853	12.786	0.577	0.477
	Text-IF[5]	63.8	(+151)	7.332	<b>5.009</b>	14.199	0.739	0.578
	Ours-teacher	40.3	(+151)	7.248	3.454	<b>20.891</b>	<u>0.743</u>	<b>0.639</b>
	Ours-distilled	4.10	-	7.279	3.328	<u>20.082</u>	<b>0.751</b>	<u>0.634</u>

Table 11: Quantitative comparison with SOTA methods on medical image fusion tasks. **Bold** and underlined values indicate the best and second-best results respectively. The additional parameters (in parentheses) are non-trainable but used during inference.

Dataset	Method	Parameters (M)	SSIM $\uparrow$	VIF $\uparrow$	$Q^{AB/F} \uparrow$	MI $\uparrow$	EN $\uparrow$
PET-MRI	PSLPT[31]	3.06	0.815	0.548	0.373	2.641	5.492
	EMFusion[32]	0.78	1.221	0.685	0.783	3.207	<b>5.646</b>
	MSRPAN[38]	0.39	1.182	0.581	<b>0.799</b>	4.119	5.073
	SwinFusion[3]	13.04	0.725	0.703	0.683	3.662	5.817
	Zero[39]	19.1	1.162	0.635	0.774	3.786	5.495
	U2Fusion[2]	0.63	0.494	0.460	0.292	2.785	5.532
	CDDFuse[27]	2.40	1.227	0.650	0.765	3.572	5.149
	Text-IF[5]	63.8 (+151)	<u>1.232</u>	0.640	0.690	3.718	5.443
	Ours-teacher	40.3 (+151)	1.223	<u>0.909</u>	0.782	<u>4.248</u>	<u>5.611</u>
	Ours-distilled	4.10	<b>1.243</b>	<b>0.929</b>	<u>0.784</u>	<b>4.318</b>	5.474
CT-MRI	PSLPT[31]	3.06	0.810	0.502	0.432	2.392	4.730
	EMFusion[32]	0.78	1.266	0.552	0.475	3.116	4.785
	MSRPAN[38]	0.39	1.261	0.436	0.455	<b>4.126</b>	4.202
	SwinFusion[3]	13.04	0.579	0.522	0.545	3.190	<u>5.144</u>
	Zero[39]	19.1	1.199	0.320	<u>0.582</u>	3.358	4.406
	U2Fusion[2]	0.63	0.042	0.074	0.489	1.694	4.896
	CDDFuse[27]	2.40	1.224	0.526	0.530	<u>3.683</u>	<b>5.733</b>
	Text-IF[5]	63.8 (+151)	<b>1.313</b>	0.542	0.561	3.211	4.356
	Ours-teacher	40.3 (+151)	<b>1.313</b>	<u>0.641</u>	<b>0.657</b>	3.246	4.462
	Ours-distilled	4.10	<u>1.312</u>	<b>0.653</b>	<b>0.657</b>	3.233	4.494
SPECT-MRI	PSLPT[31]	3.06	0.933	0.359	0.325	2.747	5.140
	EMFusion[32]	0.78	<b>1.212</b>	0.665	0.692	3.210	4.911
	MSRPAN[38]	0.39	1.153	0.525	0.560	<u>4.334</u>	4.753
	SwinFusion[3]	13.04	0.684	0.744	0.720	3.795	<b>5.401</b>
	Zero	19.1	1.180	0.582	0.681	3.564	4.997
	U2Fusion[2]	0.63	0.479	0.419	0.696	2.870	4.539
	CDDFuse[27]	2.40	1.169	0.786	0.719	4.109	4.396
	Text-IF[5]	63.8 (+151)	1.200	0.747	0.715	3.994	4.807
	Ours-teacher	40.3 (+151)	<u>1.210</u>	<b>0.888</b>	<u>0.746</u>	4.248	5.035
	Ours-distilled	4.10	1.202	<u>0.887</u>	<b>0.747</b>	<b>4.371</b>	<u>5.361</u>

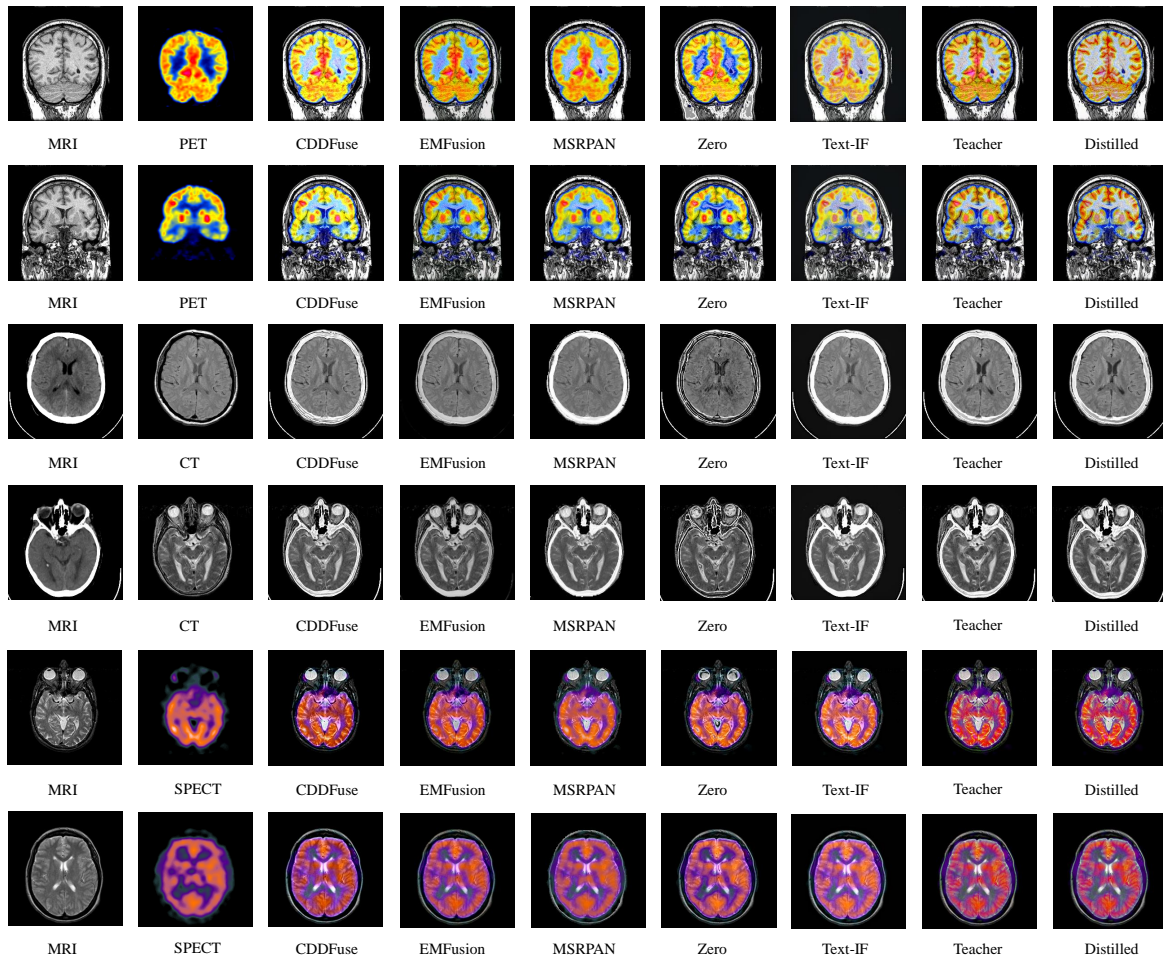


Figure 9: More compare with different methods on different datasets.